# Charge Mobility and Transport Behavior in the Ordered and Disordered States of the Regioregular Poly(3-hexylthiophene)

**Yi-Kang Lan and Ching-I Huang***

*Institute of Polymer Science and Engineering, National Taiwan University, Taipei 10617, Taiwan*

*Received: May 24, 2009; Revised Manuscript Received: September 1, 2009*

We theoretically analyze the charge-transfer behavior of regioregular poly(3-hexylthiophene) (rr-P3HT) by quantum mechanical (QM) and molecular dynamics (MD) methods. In particular, we clarify the effects associated with the respective contribution from the ordered and disordered regions. In the ordered regions, the typical value of the hole mobility along the intrachain route is about 1 $cm^2\ V^{-1}\ s^{-1}$, which is significantly larger than that along the $\pi-\pi$ interchain route, $\sim 10^{-2}\ cm^2\ V^{-1}\ s^{-1}$. Our results indicate that the main charge-transfer route within the P3HT ordered lamellae is along the intrachain direction instead of the interchain direction. Moreover, the calculated hole mobility of $10^{-2}\ cm^2\ V^{-1}\ s^{-1}$ along the $\pi-\pi$ interchain route is consistent with the experimental data measured in the P3HT single fibril. In the disordered regions, we propose a crossing-point/bridging-chain model to describe the charge-transport routes. In this model, the hole mobility can reach the limit of around $10^{-2}$ and 1 $cm^2\ V^{-1}\ s^{-1}$ when the charge takes the interchain route through the crossing points and the intrachain route along the bridging chains, respectively. As expected, the resultant mobility in the disordered state is strongly affected by the ratio of the amount of crossing points and bridging chains. When considering the presence of both ordered and disordered regions, the average overall charge mobility is mainly dominated by the charge transport in the disordered regions. The fact that some of the experimentally measured hole mobility by varying the molecular weight is limited to a maximum value of $10^{-2}\ cm^2\ V^{-1}\ s^{-1}$ is mainly due to the presence of more crossing points instead of the bridging chains in the disordered regions. With increasing the amount of the bridging chains in the disordered regions, one can expect an enhancement of the charge mobility, such as to the experimentally obtained high value of 0.1 $cm^2\ V^{-1}\ s^{-1}$.

## Introduction

Conjugated polymers continue to attract a lot of attention due to their promising applications, such as polymer light emitting diodes (PLEDs), organic field-effect transistors (OFETs), and solar cell devices. This is mainly attributed to the fact that they exhibit a unique combination of opto-electronic properties of semiconductors, easy fabrication, and low cost of manufacture.[1,2] Among these applications, understanding the charge-transport mechanism in the conjugated polymers becomes a common and important issue, as it plays a key role on the resultant performance.

Recently, particular interest has been dedicated to the highly regioregular poly(3-hexylthiophene) (rr-P3HT) as it has been shown to be among the most promising materials for OFETs and solar cell applications. Generally speaking, due to the presence of the $\pi-\pi$ interaction, these rr-P3HT chains can pack to form ordered lamellar layers so that the charge mobility can be significantly promoted within the ordered regions.[3] However, most of the polymer chains cannot 100% self-assemble orderly because of the high molecular weight. The presence of the disordered chains enables the resultant charge-transfer behavior more complicated than the small-molecule systems. Although there have been some experimental studies which have addressed the effects of molecular regioregularity, molecular weight, temperature, and processing conditions on the charge carrier mobility,[4−24] the key factors that control the charge-transfer behavior within the ordered and disordered regions need to be clarified. Herein, we aim to study the correlation between the molecular structure/packing order and charge-transfer mechanism in the P3HT systems.

Experimentally, Sirringhaus et al. reported that the self-assembled P3HT lamellae in the field-effect transistors can adopt two different orientations with respect to the substrate by tuning the molecular regioregularity and processing conditions.[4] When the P3HT regioregularity is low (81% of head-to-tail linkages), the formed lamellae in the spin-coated films are preferentially parallel to the substrate and provide a one-dimensional charge-transfer route mainly along the intrachain direction. However, in samples with high regioregularity (>91%), the ordered P3HT molecules tend to pack to form the lamellae perpendicular to the substrate, and thus the field-induced charge carriers can be transported via both intrachain and interchain ($\pi-\pi$ stacking) directions. They reported that a significant increment of the charge mobility from $10^{-4}\ cm^2\ V^{-1}\ s^{-1}$ to a value as high as 0.1 $cm^2\ V^{-1}\ s^{-1}$ can be achieved by varying the orientation of the ordered lamellae from parallel to perpendicular with respect to the substrate. This result may lead to the conclusion that the charge transport along the $\pi-\pi$ stacking interchain direction is a dominant factor in the high carrier mobility of rr-P3HT in the field-effect transistors.[5] However, varying the P3HT molecular regioregularity not only results in the different packing orientations of the lamellae (i.e., dimensionality of the charge-transfer route) but also strongly affects the chain conformation and chain packing. In addition, a few experimental studies on P3HT nanofibrils revealed that the hole

* To whom correspondence should be addressed. Phone: 886-2-33665886. Fax: 886-2-33665237. E-mail: chingih@ntu.edu.tw.

10.1021/jp904841j CCC: $40.75 
Published on Web 10/08/2009

mobility along the pure $\pi-\pi$ stacking direction (parallel to the fibril axis) is only on the order of 0.01 $cm^2\ V^{-1}\ s^{-1}$.[6−8] Thus, prior to reaching the conclusion that this enhancement of the charge mobility as large as 0.1 $cm^2\ V^{-1}\ s^{-1}$ is attributed to adding an extra transport path through the $\pi-\pi$ stacking direction, one should analyze the charge-transfer behavior along the intrachain and interchain directions, respectively.

A few studies have shown that increasing the molecular regioregularity can lead to a more rodlike (trans) chain conformation with extended $\pi$-conjugation as well as more dense packing of chains along the $\pi-\pi$ stacking direction.[9−16] For example, McCullough et al. employed molecular mechanics and ab initio calculations to examine the conformation of P3HT with different head-to-tail and head-to-head configurations.[15] They observed that the existence of head-to-head coupling significantly causes the torsional angle between two thiophene rings to deviate out of coplanarity. In contrast, the thiophene rings with a head-to-tail configuration tend to adopt a coplanar (trans) conformation, which leads to a larger value of conjugation length and red shift of the absorption spectrum. Moreover, it has also been shown that in the P3HT the torsional angle between thiophene rings is strongly associated with the alkyl side chain packing.[16] With increasing temperature, the alkyl side chains experience a conformational disordering from trans to a combination of gauche and trans and thus act as a trigger to induce the disordering in the main-chain conformation. Through the torsional rotation about the ring−ring bonds, the conjugation length can be effectively shortened. Accordingly, one cannot exclude the possibility that the more coillike chain conformation by decreasing the P3HT regioregularity and/or increasing the temperature may reduce significantly the charge-transport property along the intrachain direction, which thus also attributes to the decrease in the field-effect mobility.

Besides the molecular regularity and the chain packing orientation, various literature reported that a change in the molecular weight ($M_w$) of P3HT leads to a change in the resultant charge carrier mobility.[17−24] In particular, a significant increment of the charge mobility from $10^{-6}$ to $10^{-2}$ $cm^2\ V^{-1}\ s^{-1}$ can be reached by increasing the molecular weight.[17−21] It should be noted that since polymer chains are not 100% crystalline (well-ordered), the crystalline structure is frequently accompanied by an amorphous region. The issue that how the polymer chains fold through the ordered and disordered regions is believed to be strongly correlated with the charge-transport behavior but has not been well-understood yet. In 2004, Zen et al. investigated the effects of molecular weight and annealing of P3HT on the performance of field-effect transistors.[20] They observed that the mobility shows the same decreasing trend with increasing temperature and decreasing molecular weight. The significant blue-shift of the solid-state absorption spectra with decreasing molecular weight indicates that the P3HT backbone chains with a lower molecular weight suffer a larger distortion. Hence, the chain conformation may play a key role in controlling the charge transport in the P3HT layers.

To manifest the experimental results of the charge mobility by varying the molecular weight, some of the molecular packing models have been proposed.[21−24] For example, Zhang et al. examined the relationship between the $M_w$, the width of the formed P3HT nanofibrils, and the charge mobility.[21] They reported that the width of P3HT nanofibrils initially increases linearly with $M_w$, then levels off in the range of $M_w = 7.0-7.5$ kDa, and finally remains somewhat a constant above 10 kDa. They also observed that the charge mobility adopts a similar trend with the molecular weight, indicating that there is a strong relationship between the width of the formed nanofibrils and the charge mobility. Accordingly, they proposed that when the $M_w$ is low, the P3HT molecules may directly pack each other and the width of the nonofibril is thus equal to the length of the molecules. With increasing molecular weight (about 10 kDa), the formed nanofibrils seem to reach and remain at a maximum width of around 25 nm. Thereafter, some of the polymer chains start to disperse into the disordered regions; some act as tie molecules and bridge successive ordered nanofibrils; and some fold back to the original nanofibrils and form a loop. This model has also been proposed by Verilhac et al.[22] In 2007, Brinkmann and Rannou suggested that one may expect an increasing fraction of such bridging chains with increasing $M_w$.[23] Hence, the probability of charge transport through the less conductive amorphous zones via these bridging chains is likely to increase with $M_w$, which results in an increase of charge mobility with $M_w$. Besides, although Zen et al. observed a similar increasing trend of the charge mobility with the $M_w$, they suggested that the charge-transport properties are mainly controlled by the fraction of the formed ordered domains.[24] To clarify, when the $M_w$ is low, due to the fact that the formed ordered domains are few and isolated by the amorphous matrix, the charges are hard to transport through these ordered regions and thus the mobility is low. With increasing $M_w$, since more polymer chains pack to form ordered regions, one may expect a faster transport route for the charges through the interconnected ordered domains.

As manifested above, to thoroughly understand the charge-transfer mechanism, one should clarify the effects associated with (1) the molecular conformation in the ordered and disordered states and (2) the respective contribution/limitation of the ordered and disordered regions. Recently, we have successfully illustrated the effects of the chain conformation and chain packing on the charge-transfer behavior of rr-P3HT along the intrachain and $\pi-\pi$ interchain directions, respectively, in the ordered state via a combination of quantum mechanical (QM) and molecular dynamics (MD) simulation methods.[25] We find that decreasing the molecular regioregularity and/or increasing the temperature can cause a certain deviation degree of the thiophene rings out of coplanarity and hence a decrease in the charge carrier mobility along the main-chain direction. However, as long as the P3HT molecules remain in the ordered lamellar state due to the presence of the $\pi-\pi$ interaction, the resultant mobility along the $\pi-\pi$ interchain route is still significantly less than that along the intrachain route. Accordingly, we conclude that the main dominating charge-transport route within the P3HT ordered domains is along the intrachain direction instead of the interchain direction. In this paper we expand our modeled rr-P3HT structures by considering the presence of the disordered regions, as schematically shown in Figure 1. In particular, we consider three possible chain types in the disordered regions: extending, looping, and bridging, which have been widely suggested experimentally. We aim to analyze the contribution/limitation of the ordered and disordered zones to the resultant charge carrier mobility in the rr-P3HT systems. To our knowledge, though there have been some theoretical studies on examining the charge-transport behavior in the small-molecule systems,[26−28] our study will be the first to theoretically address the effects on the resultant charge mobility associated with the ordered and disordered polymer chains, respectively. In addition, it is worth mentioning that our calculated value of hole mobility along the $\pi-\pi$ interchain route, $10^{-2}$ $cm^2\ V^{-1}\ s^{-1}$, is consistent with the experimental value measured in the P3HT single fibril.[6−8] We find that the resultant mobility of P3HT is strongly limited to a maximum value of $10^{-2}$ $cm^2\ V^{-1}$

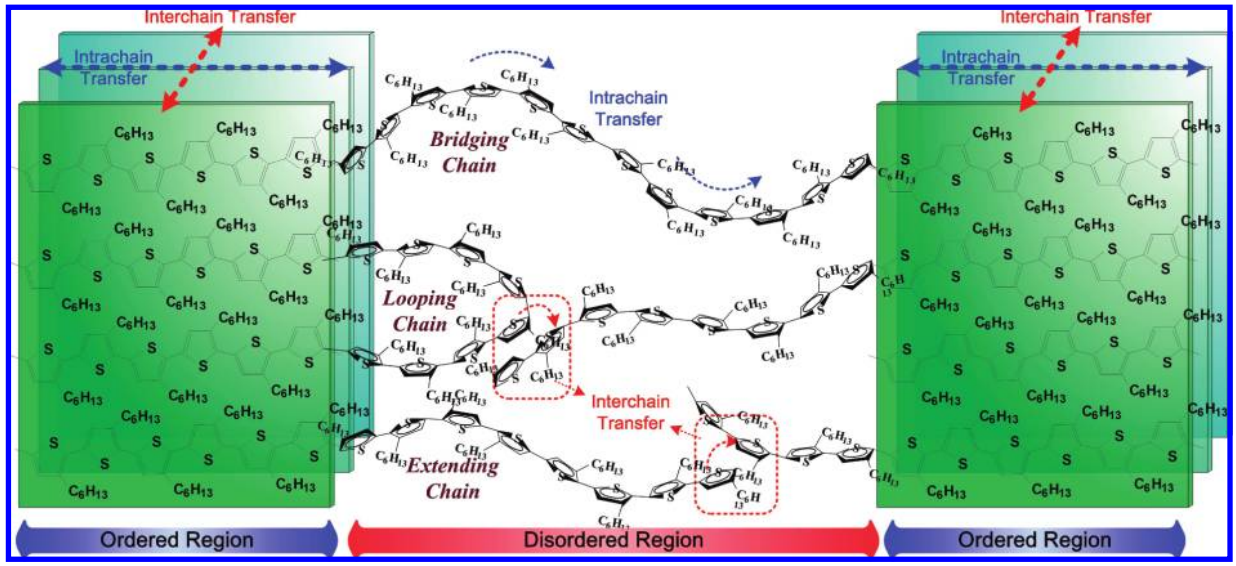


**Figure 1.** Schematic plot of the ordered and disordered chain structures of P3HT. There are three possible chain types in the disordered regions: extending, looping, and bridging chains.

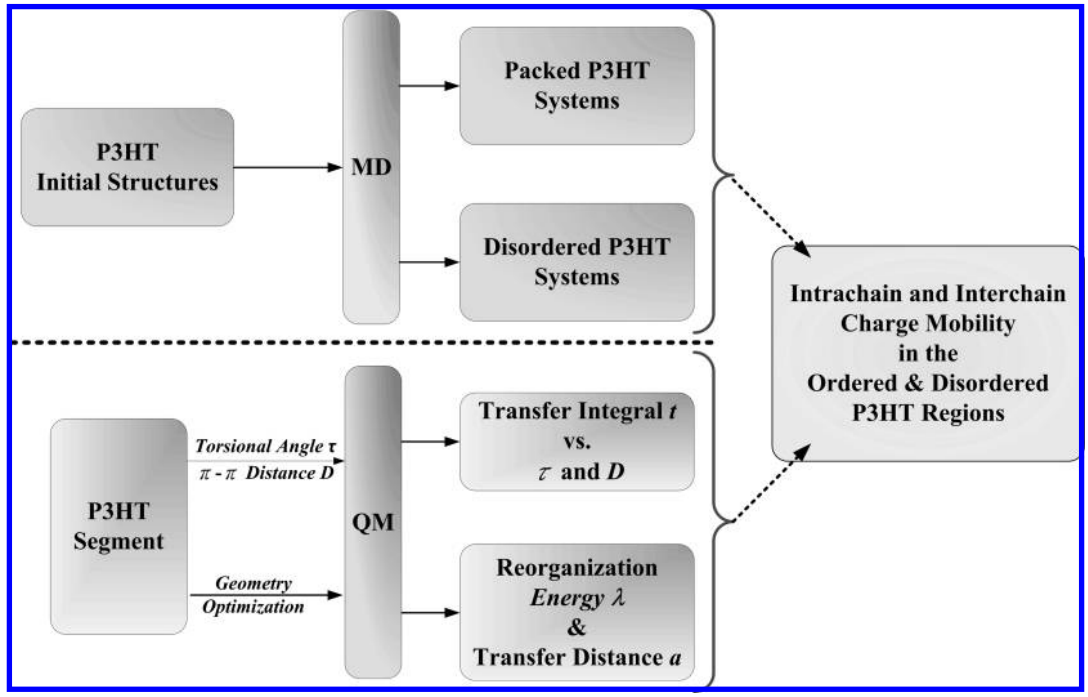


**Figure 2.** Flow chart of the simulated processes associated with the charge mobility and molecular packing structure.

$s^{-1}$ if there exist more crossing points of extending chains/loops instead of the bridging chains in the disordered regions. This finding is in excellent agreement with the experimental results of the charge mobility by varying the molecular weight.[17−19,21]

## Theoretical Methods and Systems

In this paper both QM and MD simulations are carried out to examine the charge-transport properties and the molecular conformation behavior. In Figure 2 we use a flow chart to summarize all the simulated processes incorporated here.

First, we adopt a hopping model to describe the charge-transport properties along the intrachain and interchain directions in the P3HT system. At room temperature, the motion of the carriers can be described as a sequence of uncorrelated hopping processes. In particular, we artificially vary the torsional angle between two conjugated segments ($\tau$) along the main chain to resemble the local deformation created by the molecular stereoregularity and/or temperature and calculate the transfer integral and charge mobility of both hole and electron as a function of $\tau$. For simplicity, we choose each segment as the smallest repeated unit in the main chain, i.e., two thiophene rings in a trans conformation. Note that the value of $\tau = 0°$ and 180° denotes a cis and trans conformation of the two neighbored thiophene rings, respectively. By varying the torsional angle $\tau$, how the charge carrier mobility along the main chain is affected by the local rotational degree about the ring-to-ring bonds can be manifested. In analyzing the charge-transport properties along the $\pi-\pi$ stacking interchains, we consider two segments separated by a distance $D$. Each segment also consists of two thiophene rings in a trans conformation. By varying the intermolecular distance $D$, we investigate the

influence of molecular packing on the charge mobility along the interchains.

The relationship of the carrier mobility $\mu$ and the charge-transfer rate (hopping probability per unit time) $k_{CT}$ can be obtained via the Einstein relation given as follows,[26−28]

$$\mu = \frac{ea^2}{2k_B T} k_{CT} \quad (1)$$

where $k_B$, $T$, and $e$ correspond to the Boltzmann constant, temperature, and the electronic charge. The transport distance $a$ can be obtained via an optimized model of the QM calculations.

According to the semiclassical Marcus theory,[26−29] $k_{CT}$ between the neighbored segments can be expressed as follows,

$$k_{CT} = \frac{2\pi}{\hbar^2} t^2 \sqrt{\frac{1}{4\lambda\pi k_B T}} \exp\left[\frac{-(\Delta G^0 + \lambda)^2}{4\lambda k_B T}\right] \quad (2)$$

where $\hbar$, $t$, and $\lambda$ correspond to Planck's constant, the transfer integral, and the inner reorganization energy. $\Delta G°$ is the difference of the Gibbs free energy of the system before and after the charge hopping process and is equal to zero since the segments are identical. As seen in eq 2, we need to determine the magnitude of $t$ and $\lambda$ to find $k_{CT}$ and the charge mobility.

The transfer integral of a given system is related to the energetic splitting of the electronic level, which is attributable to the segment interaction. In each of the isolated segments, the HOMO (highest occupied molecular orbital) is a $\pi$-bonding orbital delocalized over the segment with energy $\varepsilon$ of this state. When the two segments approach each other and the HOMO of each segment starts to interact, new HOMO and HOMO-1 are formed. Thus, the energetic splitting due to the segment interaction is equal to the energy difference of the HOMO and HOMO-1 in the interactive segment pairs. The transfer integral of the hole is thus given by the following,

$$t_{hole} = \frac{1}{2}\sqrt{(E_H - E_{H\text{-}1})^2 - (\varepsilon_1 - \varepsilon_2)^2} \quad (3)$$

where $E_H$ and $E_{H\text{-}1}$ denote the energy levels of HOMO and HOMO-1, respectively. Because the energy for each isolated segment is equal, that is, $\varepsilon_1 = \varepsilon_2$, eq 3 becomes

$$t_{hole} = \frac{E_H - E_{H\text{-}1}}{2} \quad (4)$$

Similarly, the transfer integral of the electron ($t_{el}$) can be obtained via the energy difference between the LUMO (lowest unoccupied molecular orbital) and LUMO+1 of the interactive segment pairs, as given in eq 5,

$$t_{el} = \frac{E_{L+1} - E_L}{2} \quad (5)$$

$\lambda$ comes from the change of the vibrational structure due to the electron gain/loss process of the segment. Figure 3 displays the schematic profile of the potential energy in terms of the coordinate of the vibrational structure $Q$ for a neutral and an ionized segment, respectively. In this plot, $E_{neu}$ and $E_{ion}$ correspond to the lowest potential energy for a neutral and an ionized segment to be at the position of $Q_1$ and $Q_2$, respectively; $E^*_{neu}$ and $E^*_{ion}$ denote the energy of the neutral and ionized segment that has lost and gained an electron, respectively. These four energy values can be obtained via the structural optimization and total energy calculation processes of quantum mechanical methods. Thereafter, the value of $\lambda$ is calculated by the following equation,[26,27]

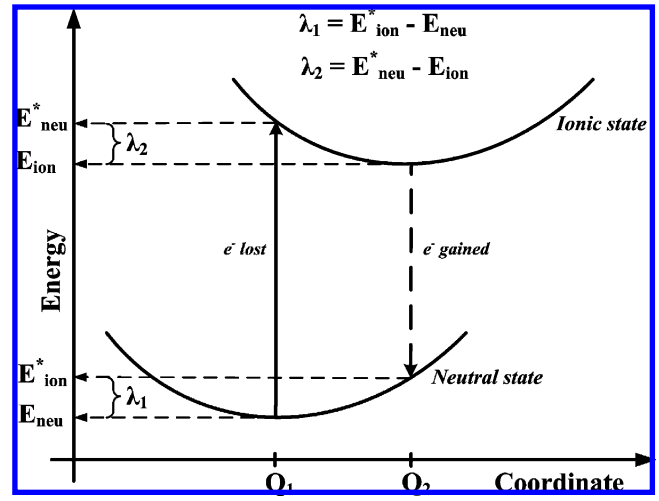


**Figure 3.** Schematic plot of the reorganization energy versus the vibration−reaction coordinate. The upper and lower curves denote the ionic and neutral state of the segment, respectively.

$$\lambda = \lambda_1 + \lambda_2 = (E^*_{ion} - E_{neu}) + (E^*_{neu} - E_{ion}) \quad (6)$$

where $\lambda_1$ and $\lambda_2$ account for the energy difference due to the structural change of gaining and losing an electron and thus equal $E^*_{ion} - E_{neu}$ and $E^*_{neu} - E_{ion}$, respectively.

All of the above electronic energy levels are carried out by using the MP2/6-311G(d,p) quantum mechanical calculations. The MP2 (Møller−Plesset second-order perturbation theory) is based on the Hartree−Fock method but includes the electron correlation terms. Hence, it is suitable to describe the long-range interactions of organic molecular pairs such as $\pi$−$\pi$ interaction.[30] To give more accurate results of the charge coupling strength along the interchain direction (coupling through space), we chose a relatively large basis set 6-311G(d,p). The 6-311G indicates that six Gaussian functions are used to describe the core orbitals, and the valence orbitals are represented by five Gaussian functions (three Gaussians in the contracted part, one in the outer part, and one in the diffuse part). The use of (d,p) polarization function attempts to describe the anisotropic charge distribution of each molecule. Since the MP2/6-311G(d,p) quantum mechanical calculation is often accompanied by huge computational time and memory resource, here we ignore the existence of the alkyl side chains, which has been shown negligible on the resultant energy level calculations. In the Supporting Information, we provide some specific values of each parameter correlated with the calculation process of charge mobility.

To examine the molecular conformation behavior of the P3HT in the ordered and disordered states, we employ the MD method with the PCFF (polymer consistent force field).[31] In simulating the ordered packing structures, we first build up a large simulation box, which contains four P3HT molecules with 16 thiophene rings per chain. Each P3HT molecule is artificially set as an infinite chain to avoid the influence of the end-group

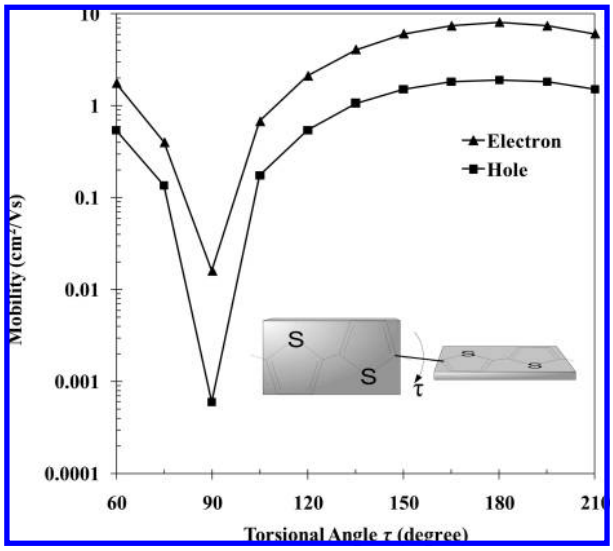


**Figure 4.** Charge mobility along the intrachain direction as a function of the torsional angle $\tau$ between the conjugated segments.

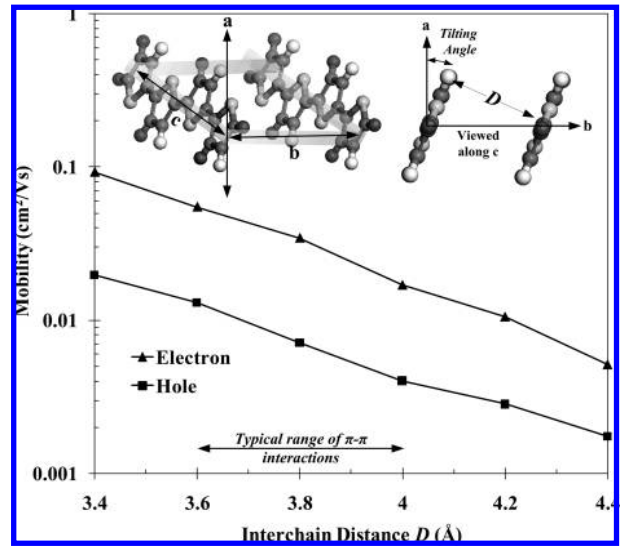


**Figure 5.** Charge mobility along the interchain direction as a function of the intermolecular separation distance $D$.

liberation.[32] To clarify, the end atom of the P3HT molecule is set to connect with the imaged chain head atom in the next periodic box. Initially the four P3HT molecules were set to form a lamellar structure with an interchain separation distance of 4.0 and 17 Å along the $\pi-\pi$ stacking and side-chain packing directions, respectively. We then adopt the steepest descent minimization method to relax and equilibrate the initial structures. The minimized system was then relaxed and followed by a series of annealing processes. The annealing temperature was first raised from 300 to 500 K at a rate of 20 K/ps and then quenched to 300 K at the same rate. This annealing cycle was repeated five times to ensure that the system had been equilibrated. Finally, it was followed by a long MD relaxation period of 1.5 ns ($1.5 \times 10^6$ time steps) at the setup temperature of each system and checked if the variation of the system temperature is smaller than 1%. After these processes were performed so that the system energy has reached the equilibrium value, then more 500 ps simulation is taken and the trajectory is collected to analyze the averaged interdistance of the neighbored chains and to get the distribution profile of the torsional angle of the neighbored thiophene rings. All the simulations were carried out in the isothermal−isobaric ensemble (*NPT*) with the time step equal to 1 fs, and the system pressure was set at $10^{-4}$ GPa (1 atm).

When simulating the molecular conformation in the disordered state, we only set one P3HT molecule with 128 thiophene rings within the simulation box. In addition, periodic boundary conditions were removed and the simulations were carried out in the canonical ensemble (*NVT*) with the time step equal to 1 fs, and the system temperature was set to 300 K. Similar annealing and data collection processes were also performed.

## Results and Discussion

Figure 4 plots the mobility of the electron and hole along the intrachain route as a function of $\tau$. As can be seen clearly, both charge carriers of electron and hole have a maximum value of mobility at $\tau = 180°$, that is, when the neighboring thiophene rings are in a trans conformation. As $\tau$ deviates from 180°, the mobility values of hole and electron decrease progressively to a minimum of $10^{-3}$ and $10^{-2}$ cm$^2$ V$^{-1}$ s$^{-1}$, respectively, when the neighboring thiophenes are located perpendicular to each other ($\tau = 90°$). Moreover, the electron mobility is larger than the hole mobility whatever the torsional angle. Recall that in the previous paper we reported that the hole-transfer integral is larger than the electron-transfer integral, which may indicate a smaller mobility of electron.[25] However, due to the fact that the segment of the thiophene dimer with an extra electron is more stable than that when an electron is lost, and thereafter has a smaller reorganization energy, the significant increment of mobility caused by a smaller $\lambda$ overcomes the decrease by a smaller $t$. If we adopt our previously simulated results via the MD method that the deviation of $\tau$ between thiophene rings out of coplanarity of 180° is about ±37° when the regioregularity decreased to 50% and the temperature increased to 500 K,[25] the resultant mobility of electron and hole along the intrachains in Figure 4 decreases from 8.1 to 4.1 cm$^2$ V$^{-1}$ s$^{-1}$ and from 1.9 to 1.1 cm$^2$ V$^{-1}$ s$^{-1}$, respectively.

To illustrate the influence of intermolecular separation, we consider two cofacial thiophene dimers, which belong to the adjacent molecules, respectively, and have the conjugated-plane tilting angle equal to 20°. The tilting angle is defined as the angle between the conjugated thiophene-ring plane and the $\vec{a}$ axis. This tilting structure at 20° has been confirmed by both theory and experiment.[25,33] We then fix the tilting angle of these two thiophene dimers at 20° and examine the evolution of the calculated charge mobility as a function of the distance $D$ in Figure 5. Similarly, the electron mobility is larger than the hole mobility no matter what the interchain distance is. Both mobilities of electron and hole show a logarithmic increase with a decrease in the interchain distance. This is mainly because of the fact that the coupling strength of p-orbitals along the intermolecular direction increases with decreasing separation distance. Accordingly, one may expect that a relatively large mobility along the interchain direction can be obtained as long as the molecules remain closer. However, a significantly large repulsive force is often accompanied with too tightly packed structures. It has been well shown that an average intermolecular distance of the ordered P3HT layers is around 3.6−4.0 Å.[3,4,25] In this typical range of the intermolecular distance, the mobility of electron and hole is limited to around 0.1 and 0.01 cm$^2$ V$^{-1}$ s$^{-1}$, respectively. In fact, the calculated value of hole mobility along the $\pi-\pi$ interchain direction, $10^{-2}$ cm$^2$ V$^{-1}$ s$^{-1}$, has been confirmed experimentally by using the P3HT single fibril as the transport layer.[6−8] In this case, the source-drain direction is

parallel to the fiber axis, which is the same as the charge-transport direction along the $\pi-\pi$ interchains.

Note that, to save the computation time, here we used the thiophene dimer as the smallest repeated unit to calculate the charge mobility. As can be seen clearly in eqs 1 and 2, the controlling factors in calculating the charge mobility are the transfer integral and the inner reorganization energy, which depend on the number of thiophene rings per segment. When considering an increase in the number of thiophene rings for each segment, because of the fact that the resonance ability which can keep the charge localized in each segment is improved, it is reasonable to expect a decrease in the transfer integral and thus a decrease in the charge mobility. While, the decrease in the inner reorganization energy for longer conjugated segments can cause an increase in the charge mobility. These two opposing effects tend to mutually cancel when we use a segment composed of three to five thiophene rings. Accordingly, the resultant charge mobility values for longer conjugated segments do not vary much with those calculated for the thiophene dimers.

In principle, our calculated mobility values represent an intrinsic property of the coupling strength between the adjacent segments, i.e., the carrier transport via the p-orbital coupling/overlapping, and the reorganization energy originated from the structure relaxation due to the charge-transfer processes. Though the calculated mobility of electron and hole in the P3HT system is predicted to be in the same order, most of the current experimental instruments cannot measure the electron mobility in the P3HT OFET devices.[1,2,34,35] This may be because of the following two practical limitations correlated with the experiments.[34] The first one is the difficulty of simultaneously providing efficient charge injection for both electrons and holes. The second one is associated with the fact that the electrons are very easily trapped within the hydroxyl groups on the surface of $SiO_2$ layers (the substrate layer). Accordingly, the experimentally measured electron mobility is frequently much smaller than the hole mobility. Recently, a modified work of Friend et al. by using a Ca drain electrode instead of the frequently used Au and/or coating a hydroxyl-free layer on the $SiO_2$ surface has shown that both the hole and electron mobility measured in the P3HT OFET are of the same order.[35]

As manifested above, when the P3HT molecules experience the $\pi-\pi$ attractive interaction and remain in the ordered lamellae, the charge mobility along the intrachain direction is significantly larger than that along the interchain direction by 2−3 orders. Therefore, to improve the charge mobility in the field-effect transistors, simply tuning up the lamellar orientation to have an additional $\pi-\pi$ transfer route may not be the key issue. One should consider the effects associated with the existence of the disordered domains and grain boundary, as most of the polymers cannot self-assemble to form 100% ordered lamellae. We thus examine the charge-transfer behavior in the disordered P3HT regions. In particular, we consider three possible chain types in the disordered regions: extending, looping, and bridging, which have been widely adopted experimentally, as shown in Figure 1.

First, the "extending" chains are defined as those which extend out of the ordered regions and end in the disordered regions. Second, the "looping" chains are those folding back to the original ordered lamellae. When the charges transfer along these two types of disordered chains, they are very likely to be trapped in the ends/loops, unless there are some other chains close enough to form the "crossing point". Thus, the charges can continue to transfer in these crossing points via the interchain transport process. As have been manifested in Figure 5, the charge mobility increases with increasing interchain distance. Due to the stability of the $\pi-\pi$ interaction, the nearest distance of the interchain $\pi-\pi$ segments of the crossing points is about 3.6 Å, and the expected hole mobility through these crossing points is limited to $10^{-2}$ cm$^2$ V$^{-1}$ s$^{-1}$.

The formation of crossing points is strongly correlated with the resultant charge mobility by varying the molecular weight of P3HT molecules. Recall that the experimental results have shown that the width of the nanorods formed by P3HT when $M_w$ is low (<10 kDa) is typically the same or slightly smaller than the length of one fully stretched P3HT molecule.[20,22] With increasing $M_w$, the width keeps increasing and finally remains somewhat a constant when $M_w$ is high (>10 kDa). One may infer that, in the very low $M_w$ region, each rod is formed by one single molecule with almost stretched conformation in the ordered lamellae and a very short tail extended to the disordered region, as schematically plotted in Figure 6. Hence, there is little chance for these short extending chains to overlap, and the charges are very difficult to transfer in the disordered regions. With an increase in $M_w$, these self-assembled P3HT molecules tend to extend more into the amorphous zones or even fold back to the original lamellae; one may expect more crossing points formed by the overlapping of these extending/looping chains. Accordingly, the probability of charge transport through the less conductive disordered zones via these crossing points is likely to increase with $M_w$, which results in an increase of charge mobility with $M_w$. If the disordered zones are full of crossing points when $M_w$ is large, these interchain segments within the crossing points are very likely to be stabilized by the $\pi-\pi$ interactions and thus have a distance of about 3.6−4.0 Å. In this case, the hole mobility can reach the maximum value of $10^{-2}$ cm$^2$ V$^{-1}$ s$^{-1}$.

In addition to the extending and looping chain types, the chains can adopt the bridging conformation in the disordered regions when they are long enough to pass from one ordered region to the next. These bridging chains can provide an intrachain-transfer route for the charge to transport across the disordered zone from one ordered region to the next. Thus, the corresponding charge mobility along the bridging chains is related to the molecular conformation of rr-P3HT in the disordered state. Figure 7 displays the converged molecular structure of one P3HT chain with 128 thiophene rings at a regioregularity value of 100% and temperature at 300 K via the MD simulation method. In the simulations periodic boundary conditions are removed, which is analogous to simulating one single P3HT chain in an infinitely large box under vacuum. It is clear that without the presence of the $\pi-\pi$ interchain interaction, the P3HT molecule in the disordered state exhibits a more coillike conformation. The distribution profile of the torsional angle between the adjacent thiophene rings, as shown in Figure 8, reveals the fact that the disordered P3HT chain has a broader degree of the $\tau$ distribution than the ordered P3HT. It is interesting to find that by vary the regioregularity from 100 to 50%, the same $\tau$ distribution region from 180 ± 40° is obtained. This suggests that the charge-transfer behavior along the disordered main-chain direction is not affected much by the molecular regularity. If we adopt the deviation of the torsional angle between the thiophene rings out of coplanarity of 180° as large as ±40°, the resultant hole mobility along the intrachain decreases slightly (∼1 cm$^2$ V$^{-1}$ s$^{-1}$), which is still significantly larger than that through the interchain-transport process by 2 orders. Due to the significant difference of the charge mobility through the crossing points and bridging chains, the ratio of

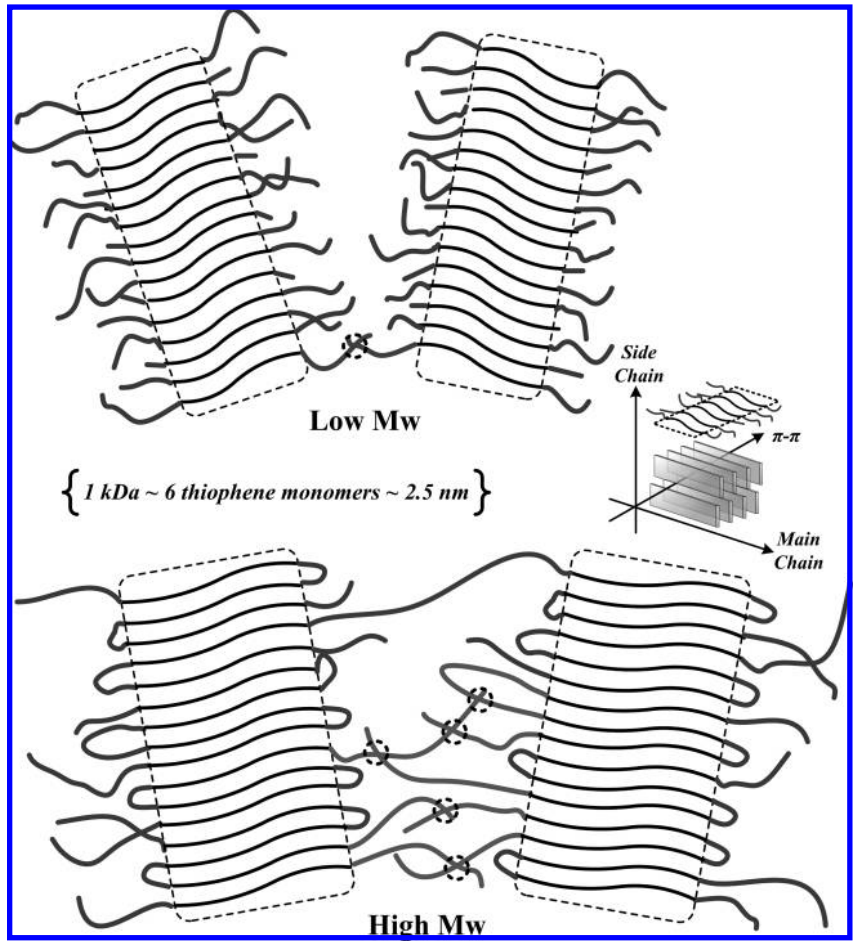


**Figure 6.** Schematic plot of the chain conformations in low and high $M_w$.

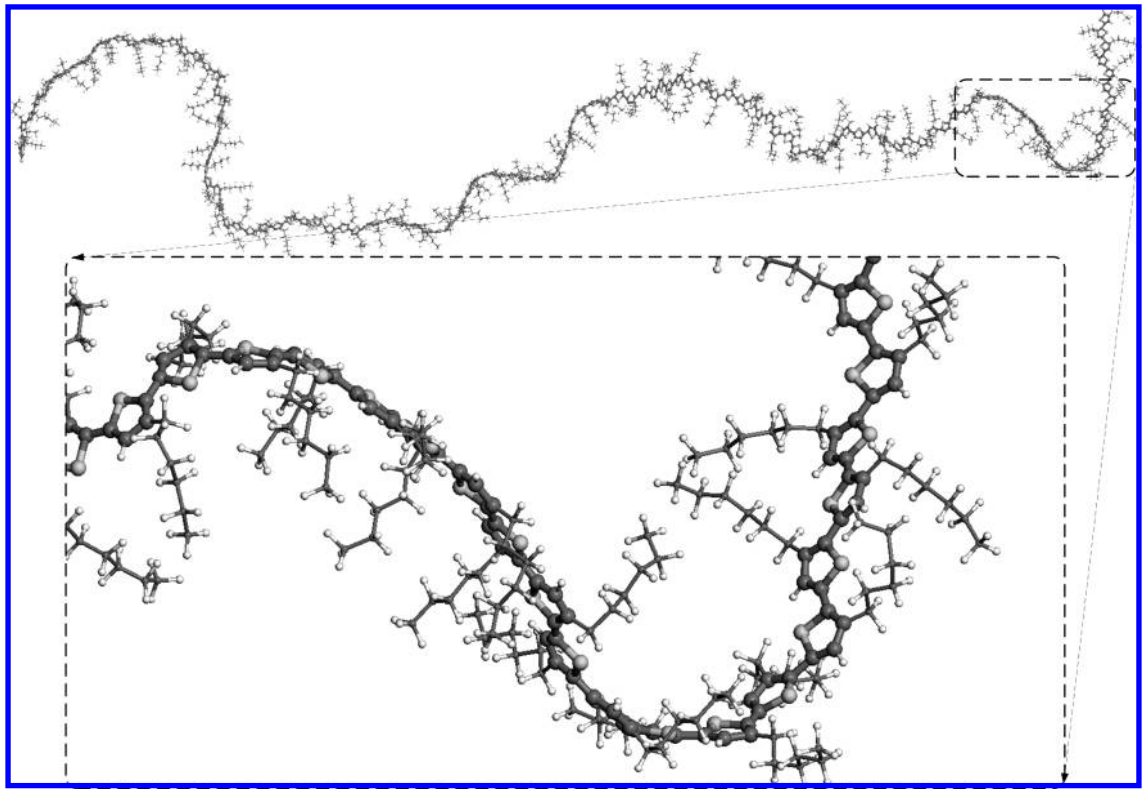

**Figure 7.** Equilibrated structure of one P3HT molecule with 128 thiophene rings per chain and a regioregularity value of 100%, simulated at 300 K via the MD method.

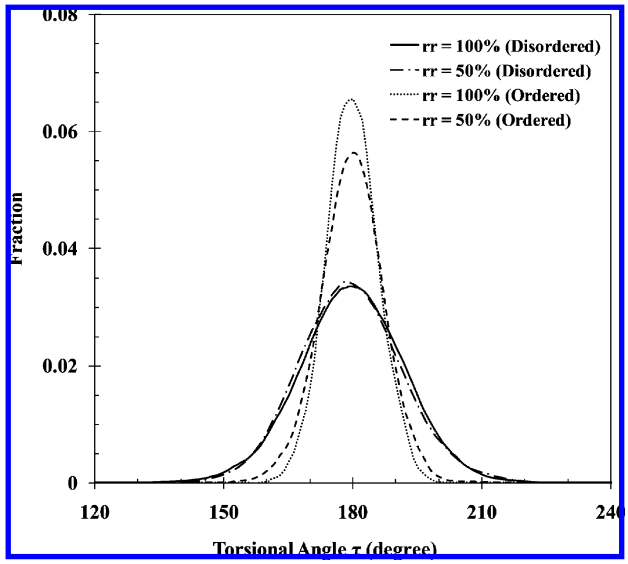


**Figure 8.** Distribution profile of the torsional angle $\tau$ between the thiophene rings for P3HT molecules at various values of regioregularity and 300 K simulated in the ordered and disordered states.

the amount of crossing points and bridging chains plays the key role in determining the average charge mobility in the disordered regions. If the disordered region is filled with the crossing points, the hole mobility is expected to be on the order of $\sim 10^{-2}$ cm$^2$ V$^{-1}$ s$^{-1}$ via the interchain-transport process. With an increasing amount of the bridging chains in the disordered region, the charge mobility increases and is expected to reach a maximum value of $\sim 1$ cm$^2$ V$^{-1}$ s$^{-1}$ if the disordered chains are all bridged.

So far, we have discussed the charge-transport behavior in the ordered and disordered regions, respectively. The remaining issue is to examine the overall charge mobility by considering the simultaneous presence of the ordered and disordered regions. For simplicity, here we ignore the effects associated with the grain boundary and assume that both the ordered and disordered domains are connected in a parallel series instead of a randomly distributed series. Hence, the average overall mobility $\mu_{av}$ can be estimated in terms of the mobility in the ordered and disordered domains, $\mu_{ord}$ and $\mu_{dis}$, by the following equation:

$$\frac{(\alpha + \beta)}{\mu_{av}} = \frac{\alpha}{\mu_{ord}} + \frac{\beta}{\mu_{dis}} \quad (7)$$

where $\alpha$ and $\beta$ denote the characteristic domain size of ordered and disordered regions, respectively. By inserting some typical values of domain size and mobility of disordered and ordered regions, how the average mobility in the P3HT system is affected could be illustrated more clearly. In the ordered lamellar domains, we choose $\mu_{ord} = 1$ cm$^2$ V$^{-1}$ s$^{-1}$, which has been shown the typical value of the hole mobility along the main intrachain route. In the disordered regions, the charge transport can adopt either the intrachain or interchain routes, depending on which chain type is in question. The value of $\mu_{dis}$ lies in a wide range from a very low value up to a maximum value around 1 cm$^2$ V$^{-1}$ s$^{-1}$. We first choose $\mu_{dis} = 0.01$ cm$^2$ V$^{-1}$ s$^{-1}$ by assuming that the disordered region is full of extending or folding types of chains so that the charge adopts the interchain-transfer process through the crossing points of $\pi-\pi$ stabilized chains. As listed in Table 1, the average mobility $\mu_{av}$ increases with increasing the ratio of domain size of ordered and disordered regions, $\alpha/\beta$. In fact, this is not surprising based on the fact that the charge transfers faster in the ordered domains. However, it is interesting to find that when $\alpha/\beta$ increases from 1/5 to 1/1, $\mu_{av}$ increases slightly from 0.01 to 0.02 cm$^2$ V$^{-1}$ s$^{-1}$, which is on the same order as $\mu_{dis}$. Even when the ratio of ordered domain size is significantly increased to 90% ($\alpha/\beta$ = 9/1), the overall mobility $\mu_{av}$ only increases to 0.09 cm$^2$ V$^{-1}$ s$^{-1}$, which is still much less than the mobility in the ordered domains of 1 cm$^2$ V$^{-1}$ s$^{-1}$. Similar behavior has been observed when $\mu_{dis}$ increases to 0.1 cm$^2$ V$^{-1}$ s$^{-1}$; the resultant value of $\mu_{av}$ varies from 0.12 to 0.53 cm$^2$ V$^{-1}$ s$^{-1}$ by varying $\alpha/\beta$ from 1/5 to 9/1. These results illustrate the fact that when the mobility in the disordered domains is significantly less than that in the ordered domains, the average overall charge mobility calculated via eq 7 is dominated by the charge transport in the disordered regions. To clarify, the disordered region, which allows the charges to move slower in a charge-transfer process, is analogous to the rate-limiting step in a chemical reaction.

**TABLE 1: Typical Values of the Average Overall Mobility (cm$^2$ V$^{-1}$ s$^{-1}$) by Varying the Domain Size and the Mobility of Ordered and Disordered Regions**

| $\alpha:\beta$ = 9:1 | | | $\alpha:\beta$ = 1:1 | | | $\alpha:\beta$ = 1:5 | | |
|---|---|---|---|---|---|---|---|---|
| $\mu_{ord}$ | $\mu_{dis}$ | $\mu_{av}$ | $\mu_{ord}$ | $\mu_{dis}$ | $\mu_{av}$ | $\mu_{ord}$ | $\mu_{dis}$ | $\mu_{av}$ |
| 1 | 0.01 | 0.09 | 1 | 0.01 | 0.02 | 1 | 0.01 | 0.01 |
| 1 | 0.1 | 0.53 | 1 | 0.1 | 0.18 | 1 | 0.1 | 0.12 |
| 1 | 1 | 1 | 1 | 1 | 1 | 1 | 1 | 1 |

Finally, we summarize our calculated results of charge mobility associated with the ordered and disordered P3HT polymer chains in Figure 9, which may guide to correlate the current experimental results in the P3HT systems. In the pure ordered lamellae, as seen in the upper part of Figure 9, there are two typical charge-transfer routes with respect to the OFET source-drain direction. If the $\pi-\pi$ interchain routes are parallel to the source-drain direction, the charge can transport via the interchain mechanism and the resultant hole mobility is in the range of $10^{-2}$ cm$^2$ V$^{-1}$ s$^{-1}$. This has been confirmed experimentally by using the P3HT single fibril as the transport layer.[6–8] Otherwise, if we have a large P3HT transport layer in which the main chains are parallel to the source-drain direction, the resultant hole mobility may reach the upper limit of the P3HT system, $\sim 1$ cm$^2$ V$^{-1}$ s$^{-1}$. When the P3HT transport layer consists of ordered and disordered regions, as denoted in the lower part of Figure 9, the average overall charge mobility is mainly dominated by the charge transport in the disordered regions based on the fact that the mobility in the disordered domains is significantly less than that in the ordered domains. If there are very few crossing points in the disordered regions, the charge transport is very likely to be trapped in the chain ends, and thus a relatively small charge mobility is obtained. By increasing the number of crossing points, the hole mobility can be improved and reach the upper limit of $\sim 10^{-2}$ cm$^2$ V$^{-1}$ s$^{-1}$ via the interchain-transfer process provided that the disordered regions are full of the crossing points of $\pi-\pi$ stabilized chains. In addition to the interchain-transfer route through the crossing points, an intrachain route via the bridging chains is also possible in the disordered domains. With an increase in the amount of the bridging chains in the disordered regions, the hole mobility significantly increases and is expected to reach a maximum value of $\sim 1$ cm$^2$ V$^{-1}$ s$^{-1}$ when the entire disordered regions are filled with the bridging chains. On the basis of these calculated results, the fact that some of the experimental results of the charge mobility by varying the molecular weight are limited to a maximum value of $10^{-2}$ cm$^2$ V$^{-1}$ s$^{-1}$ has pointed to the

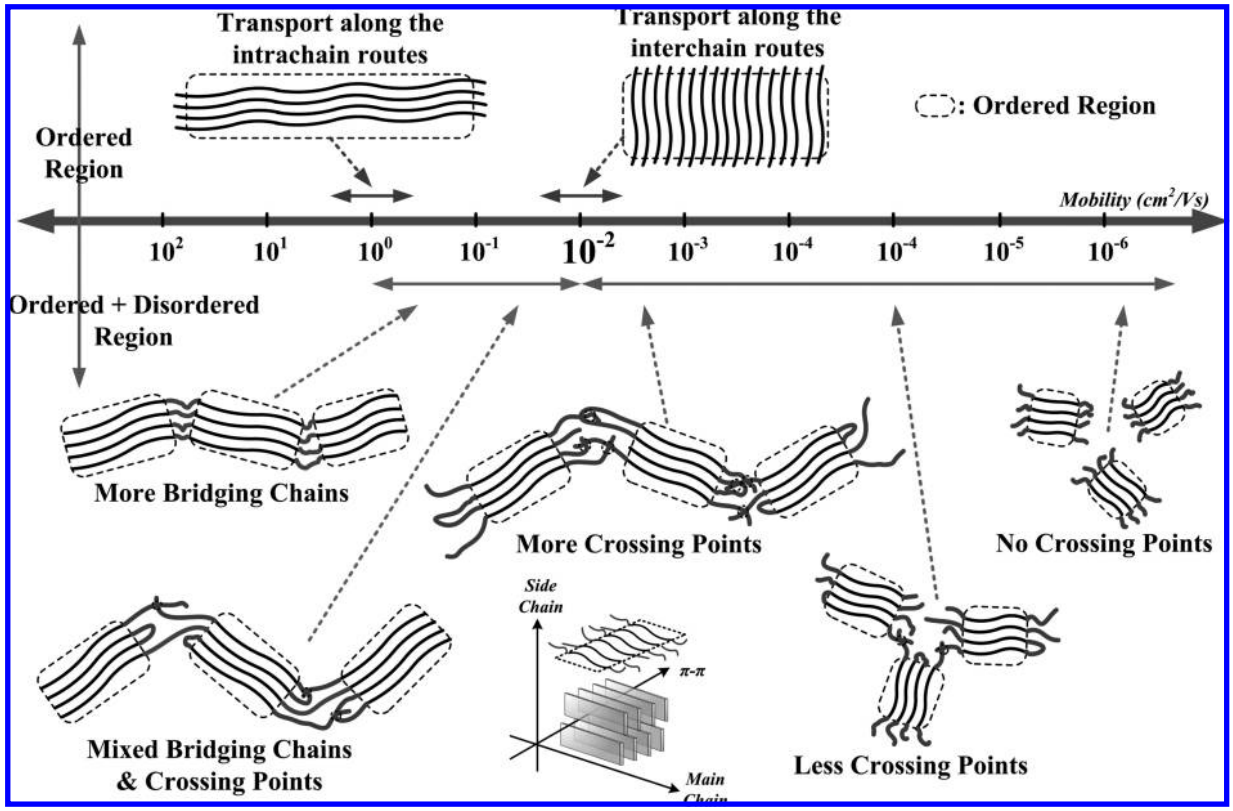


**Figure 9.** Typical region of the calculated charge mobility associated with the molecular conformation and the chain structure of P3HT in the ordered and disordered domains.

conclusion that there exist more crossing points of extending chains or loops instead of the bridging chains in the disordered regions. With an increase in the amount of the bridging chains in the disordered regions, one can expect an enhancement of the charge mobility, such as to the experimentally obtained high value of 0.1 $cm^2V^{-1}sec^{-1}$.

## Conclusions

We employed quantum mechanical and molecular dynamics methods to examine the charge-transport properties and the molecular conformation behavior of P3HT molecules in the ordered and disordered states. When the molecules experience the $\pi-\pi$ attractive interaction and remain in the ordered lamellae, the charge can adopt two transport processes along the intrachain and interchain directions. Typically, the value of the hole mobility along the intrachains is about 1 $cm^2\ V^{-1}\ s^{-1}$, which is significantly larger than that along the interchain direction of $\sim 10^{-2}$ $cm^2\ V^{-1}\ s^{-1}$ by 2−3 orders. This result illustrates that the main dominating charge-transport route within the P3HT ordered domains is along the intrachain direction instead of the interchain direction. By using the P3HT single fibril as the transport layer, our calculated mobility value $\sim 10^{-2}$ $cm^2\ V^{-1}\ s^{-1}$ has been confirmed experimentally. In the disordered domains, the charge transport can occur via the interchain route through the crossing points formed by close enough chain ends/loops or the intrachain route along the bridging chains. Due to the significant difference of the charge mobility through the crossing points and bridging chains, the ratio of the amount of crossing points and bridging chains plays the key role in determining the average charge mobility in the disordered regions. When considering the presence of both ordered and disordered regions, the average overall charge mobility is mainly dominated by the charge transport in the disordered regions, which act as a rate limiter and allow the charge to transport much slower than in the ordered domains. Accordingly, the fact that the experimentally measured charge mobility by varying the molecular weight is limited to a maximum value of $10^{-2}$ $cm^2\ V^{-1}\ s^{-1}$ is due to the presence of more crossing points of extending chains or loops instead of the bridging chains in the disordered regions.

**Acknowledgment.** This work was supported by the National Science Council of the Republic of China through Grant NSC 97-2628-E-002-001-MY3.

**Supporting Information Available:** Typical values of the parameters related to calculate the electron/hole mobility along the intrachain and interchain directions. This information is available free of charge via the Internet at http://pubs.acs.org.

## References and Notes

(1) *Organic Electronics: Materials, Manufacturing and Applications*; Klauk, H., Ed.; Wiley-VCH: Weinheim, Germany, 2006.

(2) *Printed Organic and Molecular Electronics*; Gamota, D., Brazis, P., Kalyanasundaram, K., Zhang, J., Eds.; Kluwer Academic: Boston, MA, 2004.

(3) McCullough, R. D. *Adv. Mater.* **1998**, *10* (2), 93–116.

(4) Sirringhaus, H.; Brown, P. J.; Friend, R. H.; Nielsen, M. M.; Bechgaard, K.; Langeveld-Voss, B. M. W.; Spiering, A. J. H.; Janssen, R. A. J.; Meijer, E. W.; Herwig, P.; de Leeuw, D. M. *Nature* **1999**, *401* (6754), 685–688.

(5) Sirringhaus, H.; Brown, P. J.; Friend, R. H.; Nielsen, M. M.; Bechgaard, K.; Langeveld-Voss, B. M. W.; Spiering, A. J. H.; Janssen, R. A. J.; Meijer, E. W. *Synth. Met.* **2000**, *111*, 129–132.

(6) Merlo, J. A.; Frisbie, C. D. *J. Polym. Sci., Part B: Polym. Phys.* **2003**, *41* (21), 2674–2680.

(7) Merlo, J. A.; Frisbie, C. D. *J. Phys. Chem. B* **2004**, *108*, 19169–19179.

(8) Kim, D. H.; Jang, Y.; Park, Y. D.; Cho, K. *J. Phys. Chem. B* **2006**, *110*, 15763–15768.

(9) Chen, T. A.; Wu, X. M.; Rieke, R. D. *J. Am. Chem. Soc.* **1995**, *117*, 233–244.

(10) Kaneto, K.; Hatae, K.; Nagamatsu, S.; Takashima, W.; Pandey, S. S.; Endo, K.; Rikukawa, M. *Jpn. J. Appl. Phys., Part 2* **1999**, *38* (10B), L1188–L1190.

(11) Kim, Y.; Cook, S.; Tuladhar, S. M.; Choulis, S. A.; Nelson, J.; Durrant, J. R.; Bradley, D. D. C.; Giles, M.; McCulloch, I.; Ha, C. S.; Ree, M. *Nat. Mater.* **2006**, *5* (3), 197–203.

(12) McCullough, R. D.; Lowe, R. D.; Jayaraman, M.; Ewbank, P. C.; Anderson, D. L.; Tristramnagle, S. *Synth. Met.* **1993**, *55* (2−3), 1198–1203.

(13) Pandey, S. S.; Takashima, W.; Nagamatsu, S.; Endo, T.; Rikukawa, M.; Kaneto, K. *Jpn. J. Appl. Phys., Part 2* **2000**, *39* (2A), L94–L97.

(14) Sentein, C.; Mouanda, B.; Rosilio, A.; Rosilio, C. *Synth. Met.* **1996**, *83* (1), 27–37.

(15) McCullough, R. D.; Lowe, R. D.; Jayaraman, M.; Anderson, D. L. *J. Org. Chem.* **1993**, *58*, 904–912.

(16) Tashiro, K.; Ono, K.; Minagawa, Y.; Kobayashi, K.; Kawai, T.; Yoshino, K. *Synth. Met.* **1991**, *41* (1−2), 571–574.

(17) Verilhac, J. M.; Pokrop, R.; LeBlevennec, G.; Kulszewicz-Bajer, I.; Buga, K.; Zagorska, M.; Sadki, S.; Pron, A. *J. Phys. Chem. B* **2006**, *110*, 13305–13309.

(18) Kline, R. J.; McGehee, M. D.; Kadnikova, E. N.; Liu, J. S.; Frechet, J. M. J. *Adv. Mater.* **2003**, *15* (18), 1519+.

(19) Kline, R. J.; McGehee, M. D.; Kadnikova, E. N.; Liu, J. S.; Frechet, J. M. J.; Toney, M. F. *Macromolecules* **2005**, *38*, 3312–3319.

(20) Zen, A.; Pflaum, J.; Hirschmann, S.; Zhuang, W.; Jaiser, F.; Asawapirom, U.; Rabe, J. P.; Scherf, U.; Neher, D. *Adv. Funct. Mater.* **2004**, *14* (8), 757–764.

(21) Zhang, R.; Li, B.; Iovu, M. C.; Jeffries-El, M.; Sauve, G.; Cooper, J.; Jia, S. J.; Tristram-Nagle, S.; Smilgies, D. M.; Lambeth, D. N.; McCullough, R. D.; Kowalewski, T. *J. Am. Chem. Soc.* **2006**, *128*, 3480–3481.

(22) Verilhac, J. M.; LeBlevennec, G.; Djurado, D.; Rieutord, F.; Chouiki, M.; Travers, J. P.; Pron, A. *Synth. Met.* **2006**, *156* (11−13), 815–823.

(23) Brinkmann, M.; Rannou, P. *Adv. Funct. Mater.* **2007**, *17* (1), 101–108.

(24) Zen, A.; Saphiannikova, M.; Neher, D.; Grenzer, J.; Grigorian, S.; Pietsch, U.; Asawapirom, U.; Janietz, S.; Scherf, U.; Lieberwirth, I.; Wegner, G. *Macromolecules* **2006**, *39*, 2162–2171.

(25) Lan, Y. K.; Huang, C. I. *J. Phys. Chem. B* **2008**, *112* (47), 14857–14862.

(26) Deng, W. Q.; Goddard, W. A. *J. Phys. Chem. B* **2004**, *108*, 8614–8621.

(27) Bredas, J. L.; Beljonne, D.; Coropceanu, V.; Cornil, J. *Chem. Rev.* **2004**, *104*, 4971–5003.

(28) Coropceanu, V.; Cornil, J.; Filho, D. A. S.; Olivier, Y.; Silbey, R.; Bredas, J. L. *Chem. Rev.* **2007**, *107*, 926–952.

(29) DeLongchamp, D. M.; Kline, R. J.; Lin, E. K.; Fischer, D. A.; Richter, L. J.; Lucas, L. A.; Heeney, M.; McCulloch, I.; Northrup, J. E. *Adv. Mater.* **2007**, *19* (6), 833+.

(30) Liang, C.; Newton, M. D. *J. Phys. Chem.* **1992**, *96*, 2855–2866.

(31) Tsuzuki, S.; Honda, K.; Azumi, R. *J. Am. Chem. Soc.* **2002**, *124*, 12200–12209.

(32) Sun, H. *Macromolecules* **1995**, *28*, 701–712.

(33) Yang, H. C.; Hua, C. Y.; Kuo, M. Y.; Huang, Q.; Chen, C. L. *ChemPhysChem* **2004**, *5* (3), 373–381.

(34) Sirringhaus, H. *Nat. Mater.* **2003**, *2* (10), 641–642.

(35) Chua, L. L.; Zaumseil, J.; Chang, J. F.; Ou, E. C. W.; Ho, P. K. H.; Sirringhaus, H.; Friend, R. H. *Nature* **2005**, *434* (7030), 194–199.

JP904841J